Experimental study of the rubber cord adhesion inflation test

K. Kane[a,d,*], J. Jumel[a,b,c], F. Lallet[d], A. Mbiakop-Ngassa[d], J.-M. Vacherand[d], M.E.R. Shanahan[a,b,c]

[a] I2M, University of Bordeaux, UMR 5295, F-33400 Talence, France
[b] CNRS, I2M, UMR 5295, F-33400 Talence, France
[c] Arts et Métiers Paris Tech, I2M, UMR 5295, F-33400 Talence, France
[d] Manufacture française des pneumatiques MICHELIN, Site de Ladoux, 23 place Carmes Déchaux, 63040 Clermont-Ferrand, France

Keywords:
Rubber cord adhesion
Inflation test
Hyperelasticity
Ogden model
SERR

A B S T R A C T

An important property affecting the integrity of a tyre is the adhesion between rubber and reinforcements such as metal cords. Standard tests used to evaluate rubber-metal adhesion fail to predict the intrinsic interfacial behaviour. A novel test protocol, referred to as the Rubber Cord Adhesion Inflation Test (RCAIT), has therefore been developed. In this work, RCAIT is used to compare the performance of four different adhesive systems (two rubber types and two cord coatings). In addition, the effect of fluid injection rate on crack propagation pressure is evaluated and is correlated to the sensitivity of the tensile behaviour of the rubber to strain rate. Some improvements in the RCAIT analysis are also proposed here. A thick rubber tube inflation model is proposed in conjunction with the Ogden model for hyperelastic behaviour that can be applied to other elastomeric models as well. In conclusion, the relationship between crack propagation speed and Critical Strain Energy Release Rate (SERR) is discussed.

1. Introduction

Tyres are complex structures with multiple layers of reinforcement such as fabric, polymers and, most importantly, metal cord mesh. As for laminated composites, both tyre strength and rigidity are largely controlled by properties of the cord reinforcements [1]. Ensuring strong adhesion between rubber and metal cords is therefore a key issue for developing high performance and durable tyres for automotive applications. To ensure reliable and long-lasting load transfer between cords, a strong and durable rubber-cord interface should be produced. The classic method for bonding tyre cords to rubber consists of depositing a thin layer of brass or bronze on the cord surface [2]. The cords in this case are made out of steel. During vulcanization of the rubber, copper from the coating and sulphur from the rubber react chemically to create a strong dendritic interface. However, due to aggressive environmental exposure, this interface undergoes oxidation and corrosive degradation during the life of a tyre. Therefore, it is important to assess the long-term performance of the rubber-cord adhesion. Significant developments have been made to improve rubber-cord interface performance by using alternative coating technologies or by using alloying elements. Notwithstanding the development of innovative adhesive systems, the quantitative evaluation of rubber-cord adhesion remains a challenging task. Indeed, few test protocols have been previously proposed to evaluate the interfacial strength and/or toughness of such interfaces. In a planar configuration, the rubber-metal adhesion strength is generally evaluated with peel tests using standard procedures such as those described

Nomenclature

c	integration constant	v, w	inner, outer rubber envelope radii (deformed state)
G, G_c	Strain Energy Release Rate (SERR), critical SERR	α, μ	Ogden parameters
P	fluid inflation pressure	λ_r, λ_θ, λ_z	radial, circumferential and axial stretch ratio
p	hydrostatic pressure component	σ_r, σ_θ, σ_z	radial, circumferential and axial component of the Cauchy stress tensor
R	inner radius of the confinement tube	*CIS*	Confined Inflation Stage
r, r_0	radial position- deformed, undeformed	RCAIT	Rubber Cord Adhesion Inflation Test
v_0, w_0	inner, outer initial rubber envelope radii (undeformed state)	*UIS*	Unconfined Inflation Stage

in [3–6,4,5,6]. Blister and confined blister tests have also been proposed for planar configurations [7–9]. In terms of rubber-cord adhesion (non-planar case), some tests have been proposed, the most common one being the pull-out protocol, described in the *ASTM* standard [10]. Alternatively, the pull-out test configuration was also proposed by Gent and Kaang [11]. Unfortunately, these tests suffer from various experimental artefacts, the most critical being the effect of friction at the interface, which increases the load capacity of the specimens. On a mesoscopic scale, lay-up delamination is also determined using the 180° peel test [12]. Unfortunately, in this configuration, the failure properties of the specimen are not only dependent on the rubber-cord interface but also on each individual component properties as well as the lay-up characteristics. For instance, cord plasticity drastically increases the whole system's apparent strength.

Therefore, to achieve intrinsic and quantitative characterization of the rubber cord adhesion, a new test protocol was described in a previous contribution by Kane *et al* [13] viz. the *Rubber Cord Adhesion Inflation Test (RCAIT)*. Briefly, it consists of injecting a pressurized fluid in between the rubber and the cord to provoke interface separation. The specimen is in the form of a cylindrical rubber envelope and the fractured rubber envelope expands both radially and axially due to internal pressure. To avoid rubber failure and to force the crack to propagate along the cord, a confinement tube is used. A hyperelastic description of the rubber inflation process is employed to evaluate the potential energy stored in the rubber. Finally, a global energy balance of the system is performed to evaluate the critical strain energy release rate of the crack propagation.

In this article, an improved version of the test set-up, protocol and analysis of the previous work [13] is presented. The test protocol is used to evaluate adhesive performance of different systems considering two types of rubber mixes and two types of cord coatings. In addition, the effect of fluid injection rate on the fluid pressure provoking the crack propagation is evaluated experimentally. This is correlated to the sensitivity of the rubber behaviour to strain rate. These results demonstrate the capability of the RCAIT to distinguish and quantify the adhesive performance of different rubber-metal cord systems.

2. Rubber cord adhesion inflation test (RCAIT) protocol

The RCAIT is inspired by the constrained blister test proposed in [9] and [8]. In the case of RCAIT, the rubber is deposited around a wire: the planar configuration of the blister test is thus changed to cylindrical (axisymmetric) geometry.

2.1. Test specimens and bulk rubber characterization

The RCAIT specimen is composed of a *100* mm long cylindrical rubber envelope of outer radius $w_0 = 4.7$ mm containing a brass/bronze coated steel wire of radius $v_0 = 0.65$ mm along its axis. The wire is bonded to the rubber during the vulcanization process. To ensure reproducible specimen dimensions and accurate wire alignment along the cylinder axis, a specific mould has been designed. Crude rubber is placed in the mould in which the cord is already axially aligned under a small tension. The two halves of the mould are clamped together, and the mould is placed in a furnace to produce Cu_xS bonding together with rubber vulcanization. An anti-adherent PTFE tape covers half the length of the cord to produce initial debonding (or pre-crack). In addition, specific geometric features are added to the ends of the specimen. This enables it to be clamped to the test stand. It also helps to minimise stress concentration, which can potentially cause premature failure before interfacial crack propagation occurs. Fig. 1 shows a schematic of the specimen. The debonding length (marked by white tape) is *50* mm.

The cords are made of steel and obtained using wire drawing process. Two different types of coatings (brass and bronze) are deposited on the steel cord during the wire drawing process. In actual tyres, the steel cord is brass coated: bronze coating is now obsolete. The bronze-coated specimens are therefore used in this work only for comparative purposes. Coating average thickness is in the range of *0.05 to* 0.1 μm. Two different types of rubber mixes are also considered having different mechanical and adhesive behaviour. In the following, these two rubber materials are designated as Mix A and Mix B. Mix A is a natural rubber with 60phr of

Fig. 1. RCAIT specimen schematic cross-section.

Carbon Black and 7phr Sulphur and rubber Mix B is a natural rubber with 65phr of Carbon Black and 4.5phr of Sulphur. Their detailed compositions and curing conditions remain subject to industrial confidentiality.

The material properties of these two mixes have been evaluated separately by performing tensile tests on dumbbell specimens. To obtain the tensile test specimens, *2.5* mm thickness rubber sheets are cured for vulcanization. The specimens are produced by pressing a mould, whose form and dimensions are depicted in Fig. 2(a), on the cured sheet. The specimens are attached to a *Zwick/Roell® Z010* tensile testing machine equipped with a *10KN* load cell and loaded under constant traverse displacement rate. Several displacement rates are used in the range *1* mm/min to *25* mm/min (or $4.4 \times 10^{-4}/s$ to $110 \times 10^{-4}/s$) to evaluate the influence of strain rate on the rubber mechanical behaviour. To measure elongation, white marks are drawn on the specimen. Pictures of the specimens are acquired periodically during the test and Matlab® and *ImageJ®* scripts used to determine longitudinal elongation of the specimens. The resulting *nominal* stress (calculated per unit original area) *vs nominal* strain are represented in Fig. 3 for both Mix A and Mix B and for five loading rates. The effective elongation rate for each specimen is calculated from the elongation *vs* time evolution.

Overall, rubber Mix B shows relatively low strain rate sensitivity, even at 100% strain. Rubber Mix A seems to exhibit more pronounced strain rate sensitivity as slightly stiffer behaviour is observed at higher strain rates. However, the modification of the tensile behaviour remains relatively small considering the range of strain rates tested. Also, due to limited availability of the raw material samples for this study the tests could not be repeated for each loading rate. Therefore, it is difficult to distinguish possible material/specimen variability from loading rate effect. In the present contribution, simple hyperelastic models are considered. The viscoelastic contribution is not taken into account explicitly and separate material parameters are identified for each test. The variability will account for both material properties variability and strain rate sensitivity. Several hyperelastic models can be used to describe the monotonous loading sequence of the virgin rubber, such as Mooney-Rivlin, Ogden, Yeoh or Gent.

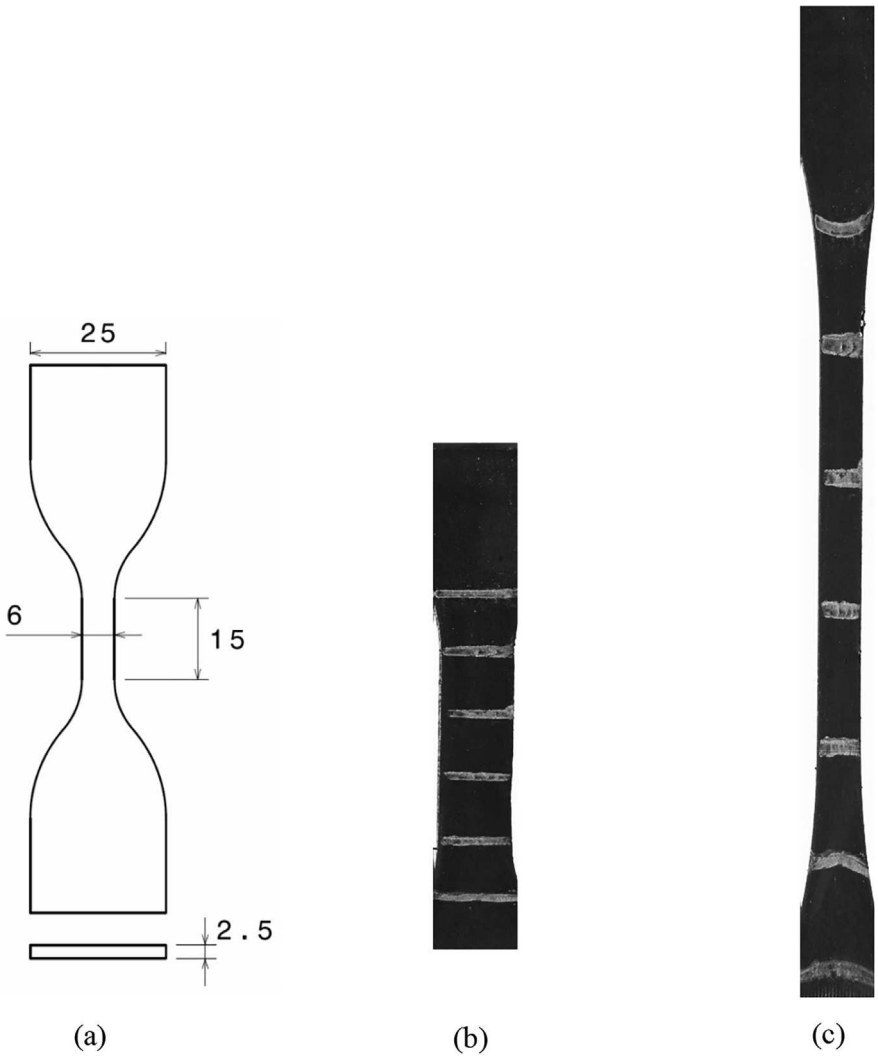

Fig. 2. (a) Geometry of the tensile test specimen (b) Tensile test specimen under no load (c) Specimen under tension.

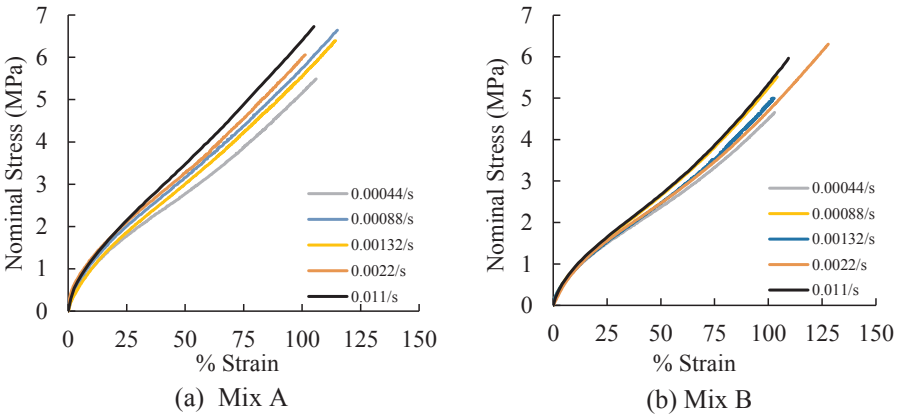

Fig. 3. Tensile test results at 5 strain rates .

Amongst these different standard models, the best fit is obtained with the Ogden model, which will therefore be used in the following analysis. Only the first order terms are needed in the series to achieve reasonable accuracy for the model, as seen in Fig. 4. The Uniaxial Cauchy Stress can therefore be given as $\sigma = \sum_{p=1}^{N} \mu_p(\lambda^{\alpha_p} - \lambda^{-\frac{1}{2}\alpha_p})$ with N = 1. As a result, the mean of the material constant values (α and μ) for rubber Mix A and Mix B in the tested strain rate range are considered. The standard deviation in the present context accounts for both specimen variability and possible strain rate effect.

The parameter α governs the rubber's behaviour at large strains (it becomes stiffer). This is because it is present as an exponent in the Cauchy stress equation. μ on the other hand, dictates overall increase or decrease in the Cauchy stress value, regardless of the strain (or stretch ratio λ). A higher value of μ thus indicates a stiffer material overall, whereas a higher value of α indicates increased stiffness at large strains. Values of α and μ for the two mixes and various loading rates are given in Fig. 5.

It is impossible to mimic the loading conditions of an inflation test on a uniaxial dumbbell specimen. The inflation test is multiaxial, and the loading histories are different along both the radial and axial directions. Therefore, in this work, average values of α and μ based on the tensile tests are used. They are: $\alpha = 2.435$ and $\mu = 2.293$ MPa for Mix A and $\alpha = 2.785$ and $\mu = 1.502$ MPa for Mix B. The variation of the rubber properties with strain rate are of use for evaluating the uncertainty in the calculation of the interfacial critical strain energy release rate (SERR) due to a poor description of the exact material behaviour. More complex envelope inflation modelling would correspond to a completely different research topic as a future prospect.

2.2. Test set-up and test protocol

The RCAIT test was used to establish SERR values, the specimen consisting of a rubber cylinder and a coaxial reinforcement cord partly bonded to the rubber tube during the vulcanization process, as described above. To enable rubber/cord separation, a pressurized fluid is injected in the gap between the two media in the debonded region in order to inflate the rubber envelope. A confinement envelope is used to limit the radial expansion of the rubber and to avoid unstable inflation as shown in Fig. 6. The specimen is fixed at the debonded end to facilitate fluid injection. A glass tube of *10* mm internal diameter is used to limit the radial

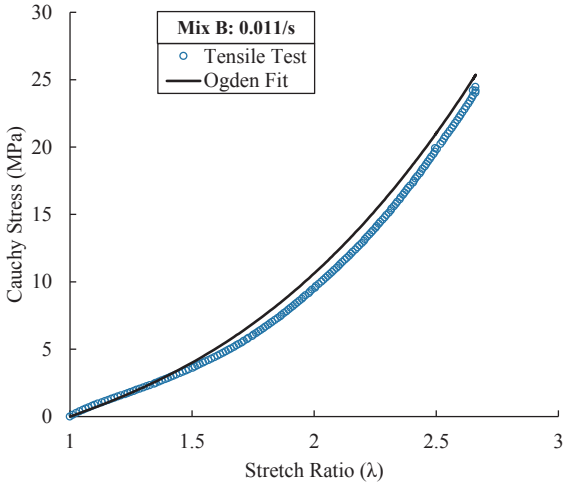

Fig. 4. Ogden Model fit for Mix B rubber uniaxially loaded at 0.011/s.

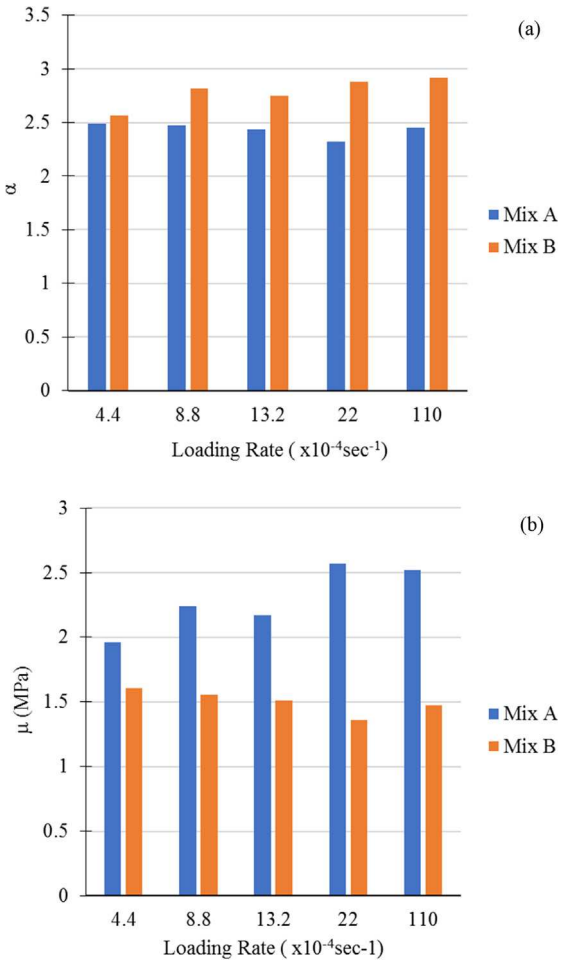

Fig. 5. Ogden Model parameters for Mix A and Mix B.

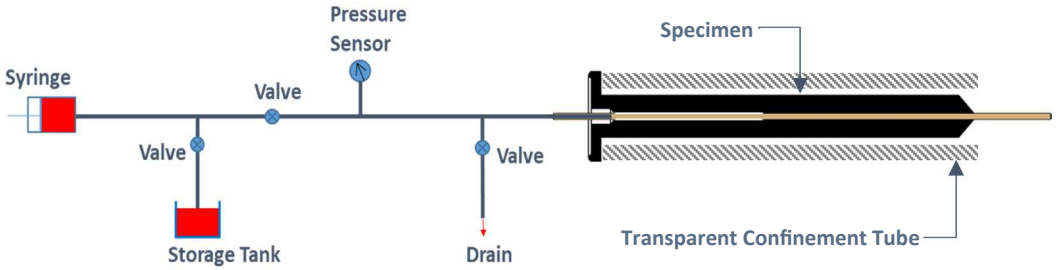

Fig. 6. Hydraulic Circuit for RCAIT.

expansion of the rubber during the experiment. The fixture is connected to a *20* ml *Swagelok®* stainless steel high-pressure syringe using hydraulic tubes, valves and connectors. The syringe is filled with the pressurizing fluid: demineralised water. A *250* bar pressure sensor (*Swagelok® Model S-Transducer*) is used to measure the injection pressure during the test. The piston of the syringe is attached to the load cell of a *Zwick/Roell® Z010* tensile testing machine. The experiments are performed under constant displacement rate of the syringe piston (or constant volume injection rate). To ease the sliding of the rubber inside the confinement tube during inflation, lubricating oil is applied in the tube prior to the experiment. The fluid pressure, force and piston displacement are recorded during the experiment with the tensile testing machine control and in-built software. A *CANON® EOS 800D* camera is used to capture images of the specimen during the experiment. During the test, image capture and pressure measurement is done simultaneously at a chosen rate by the tensile testing machine. This ensures that each data point (time, pressure, force and piston displacement) corresponds to a unique image in the camera. Multiple white spots are marked on the exterior surface of the specimen along the longitudinal direction whose positions during the experiment are monitored using a particle tracking script coded with ImageJ©. The

particle tracking assists in calculating rubber elongation (axial stretch ratio) and monitoring the crack propagation.

Before starting the test, the fluid is injected at a slow rate up to a low pressure. The drain valve is then opened to remove air trapped in the circuit, allowing the pressure to drop to zero again. The desired volume injection rate (ml/min) is converted into piston displacement rate (mm/min) and entered into the machine software. Image acquisition rate and data storage rate are also fed to the software.

As the test begins, two regimes are observed. In the first regime, the fluid pressure increases progressively, and the envelope is slowly inflated along the debonded part without any crack propagation. This is called the Unconfined Inflation Stage (UIS). As the pressure increases, the rubber envelope touches the confinement tube thereby becoming constrained at its outer diameter. Due to the radial compression of the tube and incompressible nature of the rubber, the envelope expands axially. This regime is called the Confined Inflation Stage (CIS). To ensure free axial elongation, a silicone lubrication gel is applied to the specimen and tube surfaces. Once a critical pressure is reached, fracture initiates and propagates along the rubber - cord interface. During the crack propagation stage, self-similar and stable crack propagation associated to a constant pressure is observed. Finally, unstable, catastrophic failure is observed when the crack tip approaches the end of the specimen (the conical part seen in Fig. 1). Fig. 7 shows evolution of fluid pressure during inflation of the rubber tube and subsequest crack propagation as a function of injected volume, as calculated using the crosshead displacement of the machine. Calibration of injected volume *vs* machine crosshead displacement is performed by injecting the fluid while the specimen side valve is kept closed. It was observed that the pressure increased up to *100* bar very quickly (negligible injected volume). This confirms that the overall system stiffness is sufficiently large not to influence the RCAIT results. As a result, the crosshead displacement is a reliable measurement to evaluate injected volume. The specimen in Fig. 7 is Mix A rubber bonded to a brass coated steel cord. The crack propagated at a mean pressure of *90.5* bar. It is important to note that the injection pressure is not controlled, instead the rate of injection (volume) is controlled and pressure is recorded.

2.3. Crack propagation monitoring

To evaluate the fracture energy of the interface (or critical SERR), a simple energy balance analysis was proposed assuming self-similar propagation and considering hyperelastic behaviour of the rubber [13], (see Fig. 8). Using the standard definition of SERR, fracture energy can be calculated from the experimental data as well, as shown below.

The quantities directly measured or calculated from RCAIT are fluid pressure, injected fluid volume, elapsed time and axial extension of the tube (or axial stretch ratio). From a practical perspective, measurement of fluid pressure is straightforward. It is done by simply recording the voltage output from the pressure sensor. The injected volume and elapsed time during the test are also readily found.

Monitoring crack propagation is delicate since the separation front is hidden due to the axisymmetric nature and opacity of the specimen. Crack propagation is therefore monitored by constructing a simple model of the specimen deformation. It is assumed that the extent of the process zone around the crack tip is negligible. Then, the displacement of the tip of the specimen (un-inflated end) is simply equal to:

$$d = (\lambda_z - 1)a$$

where d is the displacement of the specimen tip (or the topmost marker in Fig. 9), λ_z is the axial stretch ratio of the inflated part of the specimen and a is the crack propagation length (excluding the initial debonded length). The displacement d, is measured as soon as the crack has reached the first marker in the adhering region. Therefore, the crack propagation length is zero in the inflation regime of Fig. 10.

Considering purely hyperelastic behaviour of the rubber envelope and constant pressure self-similar crack propagation, two

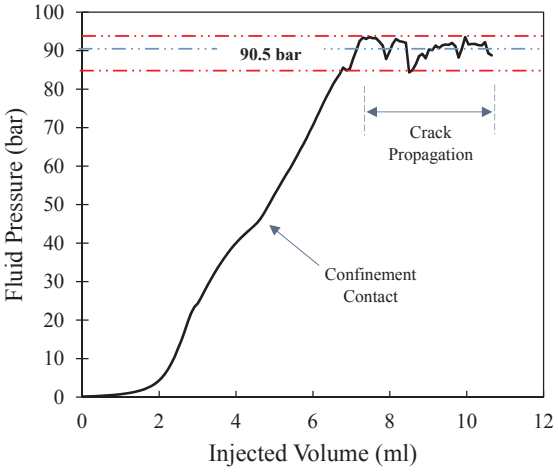

Fig. 7. RCAIT of Mix A-brass coated cord. Average crack propagation pressure is 90.5 bar.

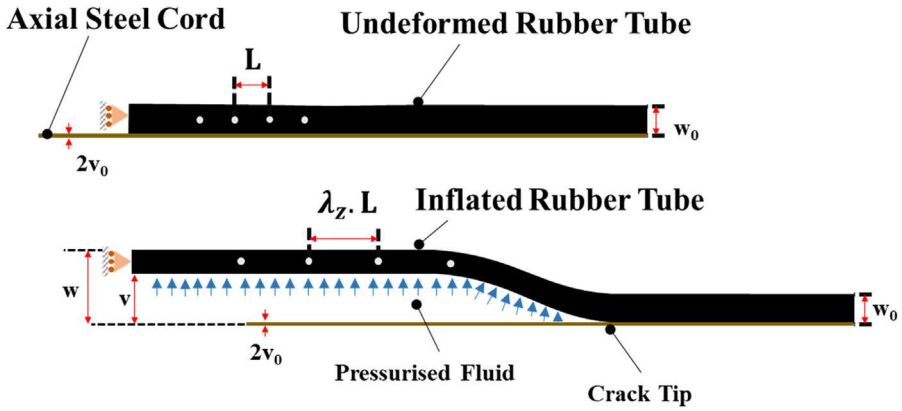

Fig. 8. Marker monitoring technique used for axial stretch ratio measurement during specimen inflation.

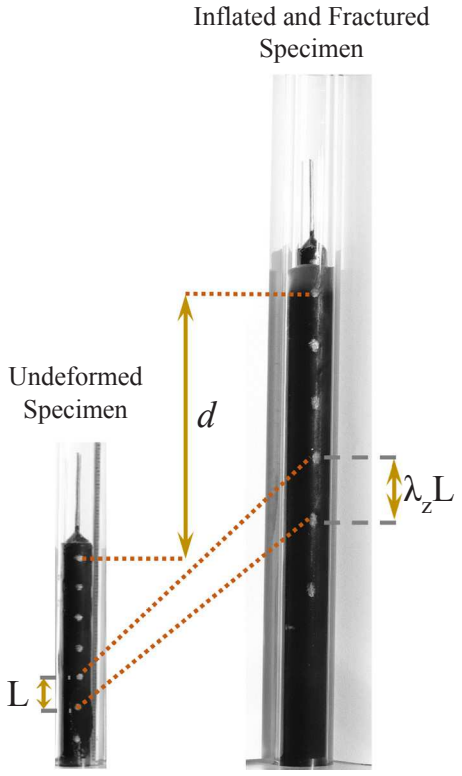

Fig. 9. Calculating axial stretch ratio (λ_z) and specimen tip displacement 'd' using marker-monitoring algorithm.

regimes can be considered. During the inflation regimes (both UIS and CIS), crack length a remains constant (zero) and λ_z can be evaluated from the specimen end displacement (see Fig. 8). During the crack propagation regime, since the inflation pressure remains constant, so does λ_z, therefore the crack propagation increment, δa, is determined from the relation:

$$\delta a = \frac{\delta d}{\lambda_z - 1}$$

To ensure reliable measurement of λ_z, marks are also drawn on the pre-cracked part of the specimen so that λ_z is measured during the specimen inflation regime. This measurement is likely to be unaffected by the process zone development near the artificial crack tip region (Fig. 9). It is important to note that the exact time of the crack initiation is not necessary in this analysis as the propagation is self-similar. The key factor is the increment of crack propagation distance δa between two points in time. These time points can be arbitrarily chosen during the crack propagation regime.

Using the crack propagation length calculated with this method, critical SERR can be calculated from the experimental results following the definition of energy release rate. The fluid pressure energy, ΔE, supplied for an arbitrary length of crack propagation,

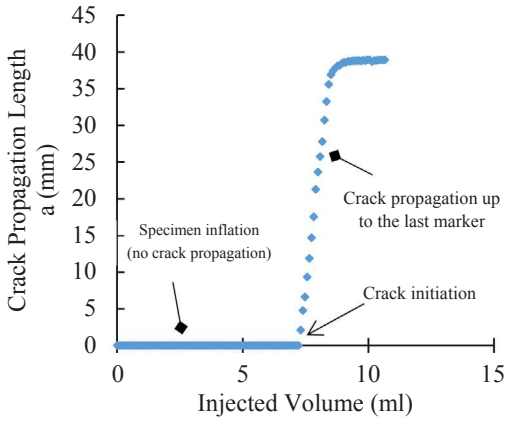

Fig. 10. Crack propagation monitoring until it reaches the last marker.

Δa, is

$$\Delta E = P\Delta V$$

where P is the average crack propagation pressure and ΔV is the fluid volume injected during propagation of Δa. This energy is partly stored in the inflated rubber (ΔE_r) and partly released during creation of fracture surface $2\pi v_0 \Delta a$, where v_o, is the inner, initial rubber envelope radius. Critical SERR is therefore:

$$G_c = \frac{P\Delta V - \Delta E_r}{2\pi v_0 \Delta a}$$

The specimen interface critical SERR can then be determined semi-analytically from the measured value of the inflation pressure using a *Thick Rubber Tube Inflation Model* as proposed in [13]. For a hyperelastic rubber with strain energy density W, ΔE_r is defined as

$$\Delta E_r = \lambda_z \Delta a \int_v^R 2\pi r W dr$$

where v is the deformed inner radius of the rubber tube and R is the confinement tube inner radius. For the Mix A-brass specimen (Fig. 7) with the Ogden model, using the material properties described in Section 2.1, ΔE_r is calculated to be *17.8* J. Therefore, the critical SERR for Mix A-brass specimen is *80.2* kJ m^{-2} for an injection speed of *1* ml/min.

One important reason for developing the theoretical model is to allow for the sensitivity of the image processing to various experimental conditions, such as the effect of lighting, that of glare from the confinement tube and various others. These factors affect the accuracy of image processing as well as the time required to perform it and are difficult to control and/or eliminate. However, the critical SERR and crack propagation length calculated with image processing provide a basis for comparison.

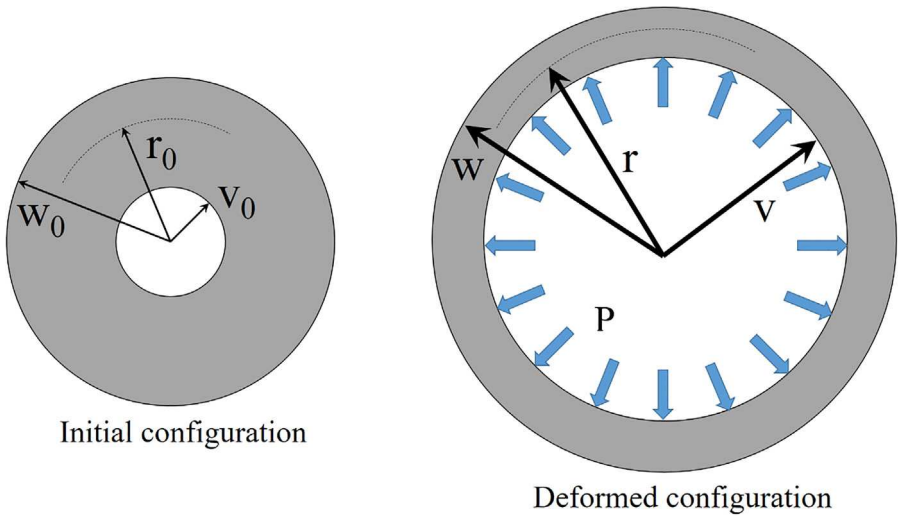

Fig. 11. Rubber tube deformation stages. P is the fluid pressure.

2.4. Thick rubber tube inflation model

In reference [13], a Mooney-Rivlin rubber model was used; however, in the present work the Ogden model is used since it reproduces the results from the uniaxial tensile tests more accurately. The constitutive equations of the *Thick Rubber Tube Inflation Model* and the solution method are derived below.

Constitutive Equations:

We consider a thick, hollow, elastomeric tube with inner and outer radii of v_0 and w_0 respectively (Fig. 11). In the deformed configuration, the radii become v and w. Due to the axisymmetric configuration, the radial and circumferential stretch ratios are given by:

$$\lambda_r = \frac{dr}{dr_0}\lambda_\theta = \frac{r}{r_0} \tag{1}$$

r_0 and r being the radial position in the initial state and deformed state respectively. Taking into account the incompressible nature of the material with the relation $\lambda_r\lambda_\theta\lambda_z = 1$ and assuming a constant axial stretch, λ_z, throughout the thickness, the general expressions for radial and circumferential stretch ratio are [14]:

$$\lambda_r{}^2 = \lambda_z{}^{-1}\left[1 - \frac{1}{cr^2}\right]\lambda_\theta{}^2 = \lambda_z{}^{-1}\left[\frac{cr^2}{cr^2 - 1}\right] \tag{2}$$

with c being an integration constant to be determined from boundary conditions together with axial stretch ratio, λ_z. The following relations give three-dimensional Cauchy stresses for an Ogden rubber:

$$\sigma_z = p + \mu\lambda_z^{\alpha} \tag{3}$$

$$\sigma_r = p + \mu\lambda_r^{\alpha} \tag{4}$$

$$\sigma_\theta = p + \mu\lambda_\theta^{\alpha} \tag{5}$$

μ and α being the Ogden the rubber coefficients (Fig. 5) and p the hydrostatic pressure due to incompressibility (not to be confused with fluid pressure P). The equilibrium equation for an axisymmetric loading is

$$\frac{d\sigma_r}{dr} + \frac{\sigma_r - \sigma\theta}{r} = 0 \tag{6}$$

Then, substituting (3)–(5) into (6) we get

$$\frac{dp}{dr} = -\mu\left[\frac{\lambda_r^{\alpha} - \lambda_\theta^{\alpha}}{r} + \alpha\lambda_r^{\alpha-1}\frac{d\lambda_r}{dr}\right] \tag{7}$$

Boundary Conditions:

During the Unconfined Inflation Stage (UIS), the rubber tube expands freely both radially and axially. Since the specimen is closed at both ends (fixed at one end and adhering to the cord at the other), an axial force is also exerted on the envelope by the internal pressure leading to the three mathematical conditions as follows:

$$\sigma_{r|(r=v)} = -P \tag{8}$$

$$\sigma_{r|(r=w)} = 0 \tag{9}$$

$$\int_v^w \sigma_z(r)2\pi r dr = P\pi v^2 \tag{10}$$

P is the pressure imparted by the injected fluid. The steel cord is not clamped and can move axially freely under the axial force given by *(10)*.

Using equations *(4) and (8)* the hydrostatic pressure p can be calculated at the inner radius (v) of the inflated rubber tube. Similarly, p can be calculated at the outer radius (w) using Equations *(4) and (9)* for UIS.

$$p_{|(r=v)} = p_v = -P - \mu\left[\frac{cv^2 - 1}{\lambda_z cv^2}\right]^{\frac{\alpha}{2}} \tag{11}$$

$$p_{|(r=w)} = p_w = -\mu\left[\frac{cw^2 - 1}{\lambda_z cw^2}\right]^{\frac{\alpha}{2}} \tag{12}$$

For CIS, the boundary condition *(9)* is changed to

$$w = R \tag{13}$$

R being the inner radius of the confinement tube. Eq. *(13)* can be used to write c in terms of λ_z (see *Eq. (25)* in [14] for intermediate steps) as

$$c = \frac{\lambda_z}{\lambda_z R^2 - {w_0}^2} \tag{14}$$

The inflation behaviour of the rubber tube can be described for an Ogden rubber by solving Equations *(8)–(10)* for UIS and *(8)–(10)* with *(14)* for CIS. By solving the equations to get λ_z, rubber tube deformation and Cauchy stresses can be calculated. It will be used further to calculate the energy stored in the inflated rubber.

Solving for λ_z:

While semi-analytical solutions were found for the UIS and CIS configuration ([14,13]), a numerical resolution technique is preferred here for the sake of simplicity and also to make the procedure adaptable to other types of rubber models. A step-by-step numerical solution is found, by considering an incremental increase of the internal radius and determining the hydrostatic pressure *p (r)*, so that boundary conditions *(8)–(10)* and *(9)* or *(14)* are satisfied. The numerical procedure is summarized in Fig. 12. The same procedure can be followed for any rubber model if the equations for three-dimensional Cauchy stresses (*(3)*, *(4) and (5)*) are known.

The reason to choose the deformed inner radius *v* as the driving parameter for the algorithm can be deduced from Fig. 13. The easiest parameter to measure during the experiment is the fluid pressure. Therefore, it is logical to keep *P* as the driving parameter in the algorithm. However, it is possible that the rubber tube inflation will become unstable due to either a large confinement radius or absence of a confinement tube. In certain cases, this may result in decreasing fluid pressure [15] or nearly constant fluid pressure, as seen in Fig. 13. In such a case, keeping *P* as the driving parameter will lead to erroneous results. Similarly, in certain cases it is possible that the axial stretch ratio of the rubber tube, λ_z, will initially decrease below unity, i.e., retraction occurs. This depends on the properties of the rubber (or the model). The inner radius *v* is the only parameter that consistently, monotonically increases during inflation.

In the UIS regime for Mix B (see Fig. 13), the rubber tube will undergo unstable inflation giving rise to aneurysms. After the point $P \sim 46.1$ *bar* ($\lambda_z \sim 2.1$) the gradient of the curve stays very close to zero. However, by choosing a tight confinement tube, i.e. smaller radius, *R*, higher pressures can be attained whilst maintaining stable inflation. Such a situation is shown in Fig. 13. The confinement

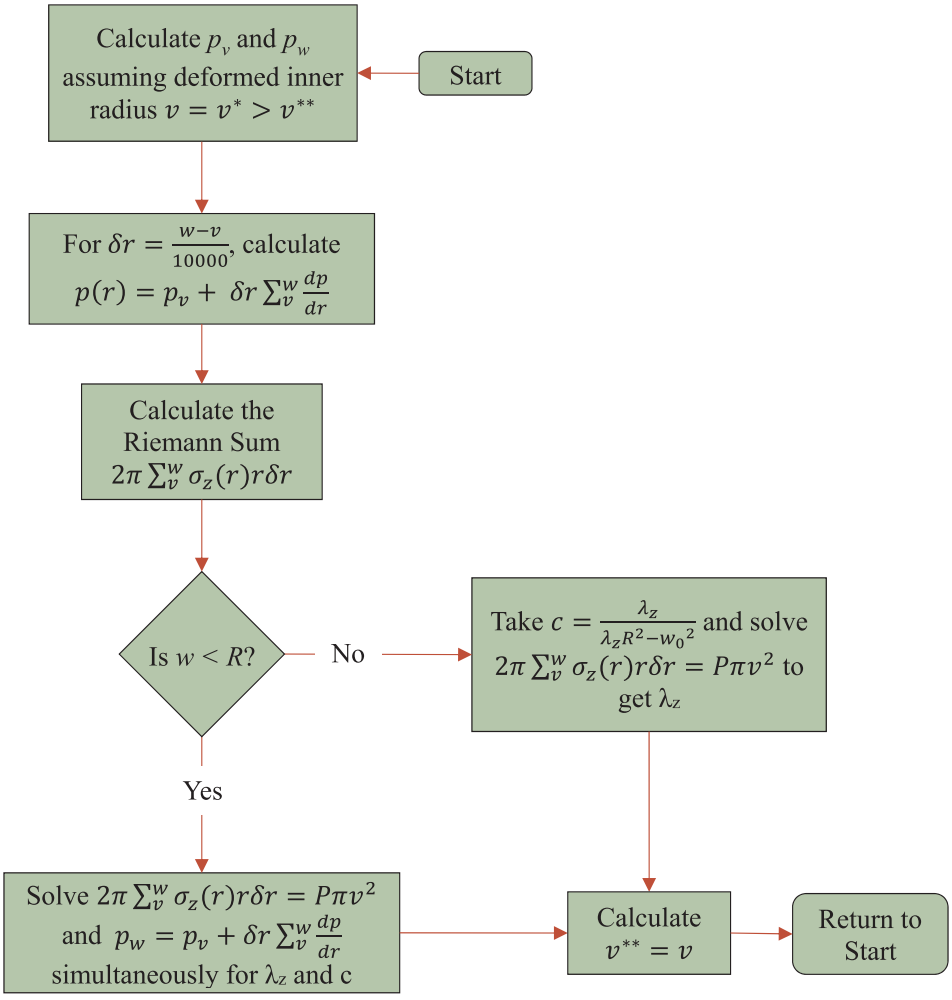

Fig. 12. Algorithm to solve the Thick Rubber Tube Inflation problem for Ogden Model.

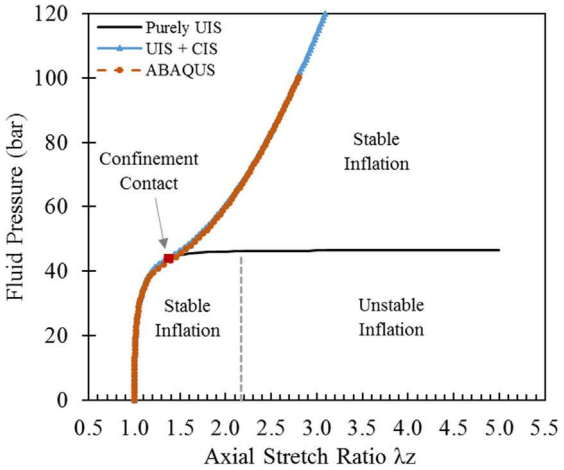

Fig. 13. Stable Inflation of an Ogden Rubber tube in the presence of a confinement. Theoretical and FE model follow very precisely the same curve.

contact occurs well before the instability point and inflation stays in a stable region even for a very large axial stretch ratio.

Thick rubber tube inflation can also be modelled in ABAQUS using the same Ogden parameters and specimen dimensions. It can be seen that the theoretical model and FE model follow very precisely the same curve. However, the theoretical model provides greater flexibility over the FE model when it comes to changing the inflation parameters such as can be extended to compute SERR for a given fluid pressure in just a few lines of code. Another advantage of the theoretical model over the FE model is the time required for convergence. Where the theoretical model can compute the curve shown in Fig. 13 in matter of few minutes, with the FE model takes nearly one hour.

2.5. SERR: Global energy balance

In [13], the equation for SERR (*Eq. (25)*) was calculated for a Mooney-Rivlin rubber. The general procedure followed is similar for any type of elastomeric material. By performing an energy balance of the system, the SERR can be calculated as following:

$$W = \Delta U_e^{fluid} + \Delta U_e^{rubber} + D \tag{15}$$

W being the energy supplied to the system by the pressurized fluid. ΔU_e^{fluid} is the energy stored due to fluid compressibility. Both quantities can be calculated in exactly the same way as described in [13]. ΔU_e^{rubber} is the energy stored in the deformed, inflated rubber and D is the energy released during crack propagation. In this work, the SERR equation is derived for an Ogden rubber with two coefficients (μ and α). The strain energy density function for an Ogden rubber(W_e)can be written as:

$$W_e = \frac{\mu}{\alpha}(\lambda_z{}^{\alpha} + \lambda_r{}^{\alpha} + \lambda_\theta{}^{\alpha} - 3) \tag{16}$$

Therefore, the energy stored in the crack length, δa, of the rubber can be written as:

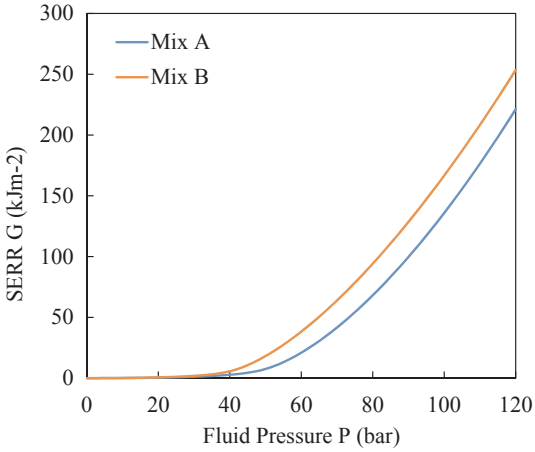

Fig. 14. G *vs* P for rubber Mix A and Mix B. α and μ are taken as average values from the tensile tests.

$$\Delta U_e^{rubber} = \lambda_z \delta a \int_v^w 2\pi r \delta w_e dr \tag{17}$$

Using the *Thick Rubber Tube Inflation Model* described earlier, λ_z, c, v and w can be calculated for the crack propagation pressure observed during RCAIT. The integration can then be done numerically by converting it into a Riemann Sum.

For an infinitesimal crack length, δa, the energy released during fracture is:

$$D = G.\ 2\pi v_0 \delta a \tag{18}$$

Therefore, the SERR can be calculated from equations *(15)*, *(17) and (18)* as:

$$G = \frac{\lambda_z P(v^2 - v_0^2)}{2v_0} - \frac{P^2 \lambda_z (v^2 - v_0^2)}{2\chi v_0} - \frac{\lambda_z}{2\pi v_0}\left[\int_v^w 2\pi r \delta w_e dr\right] \tag{19}$$

Using the *Thick Rubber Tube Inflation Model* described earlier (Fig. 12), λ_z can be calculated for a given value of P. G is therefore a function of fluid pressure (P), rubber material coefficients (μ and α) and specimen dimensions. It is independent of the initial crack length, which is consistent with the self-similar nature of the crack propagation and constant pressure measured during the test. Fig. 14 shows G *vs* fluid pressure P for both Mix A and B. The Ogden parameters are calculated as average values from the tensile tests at five loading rates (see *Section 2.1*). For pressures up to *30* bar, G is nearly the same for both rubber mixes. For the case shown in Fig. 7, the crack propagated at an average pressure of *90.5* bar. The critical strain energy release rate (G_c) is therefore *100.6 kJm*$^{-2}$.

Material nonlinearity as well as large deformation during inflation result in nonlinear behaviour of G. Comparing Fig. 14 in this work to the *SERR vs* P_i curve in [13] (Fig. 11); it is evident that calculation of G is sensitive to the quality of fit of the rubber model. In [13] for rubber Mix B bonded to brass coated steel, the crack propagation pressure was recorded as *66.6* bar and using a Mooney-Rivlin Model, G_c was found to be *15.6* kJ m^{-2}. However, fitting an Ogden model to the same rubber mix results in a G_c value of *54.7* kJ m^{-2}. Since a significant amount of the work provided by the fluid injection is transferred to the rubber, it is important to identify properly its mechanical behaviour to achieve better accuracy in the calculation of G_c.

The effect of strain rate on the calculation of G is clear from Fig. 15. As in the tensile test results shown in Fig. 3, there is considerable spread in the curves, especially at higher crack propagation pressures.

3. Rubber cord adhesion performance characterization

To investigate various experimental conditions such as volume injection rate, crack propagation rate and strain rate on rubber inflation behaviour, 20 tests were carried out. The test campaign included two rubber types – Mix A and Mix B, two cord coatings – brass and bronze, and five volume injection rates – *0.1* ml/min to *5* ml/min. As previously in Fig. 7, nearly constant inflation pressures were measured for each specimen and inflation rate during the crack propagation regime. The critical pressure varies depending on the type of specimen and inflation rate, despite the rubber behaviour itself being less sensitive to elongation rate. Any effect of loading rate on the fracture behaviour could therefore be mainly due to the behaviour of the interface viz. viscous dissipation, fluid penetration at the interface etc. Axial stretch ratio and crack propagation during the inflation tests were calculated for each case using the image-processing algorithm explained previously.

3.1. Test results

The pressure–volume evolution for Mix A is represented in Fig. 16 for bronze and brass coated steel. Fig. 17 shows similar evolution for Mix B. The effect of volume injection rate or loading rate is can be seen in the figures. Higher loading rates (or injection rates) cause greater energy dissipation in the rubber and particularly near the crack tip, allowing the pressure to mount higher before

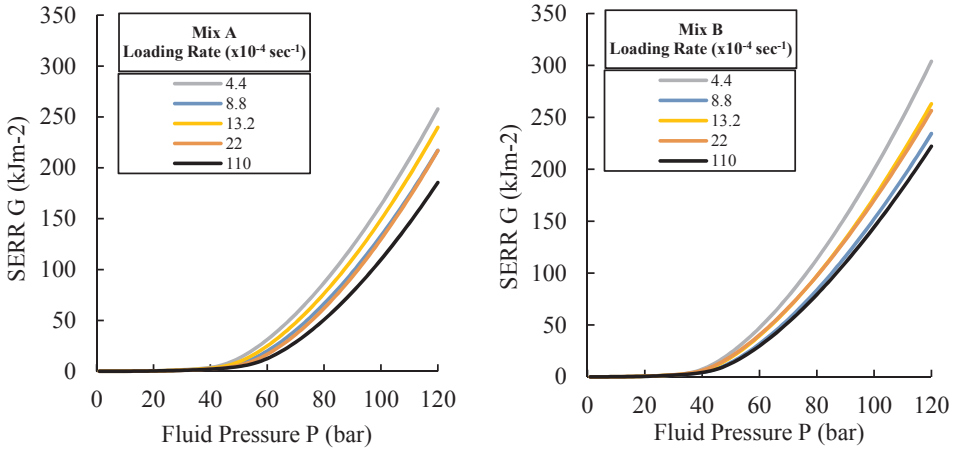

Fig. 15. Effect of rubber properties (loading rate) on G.

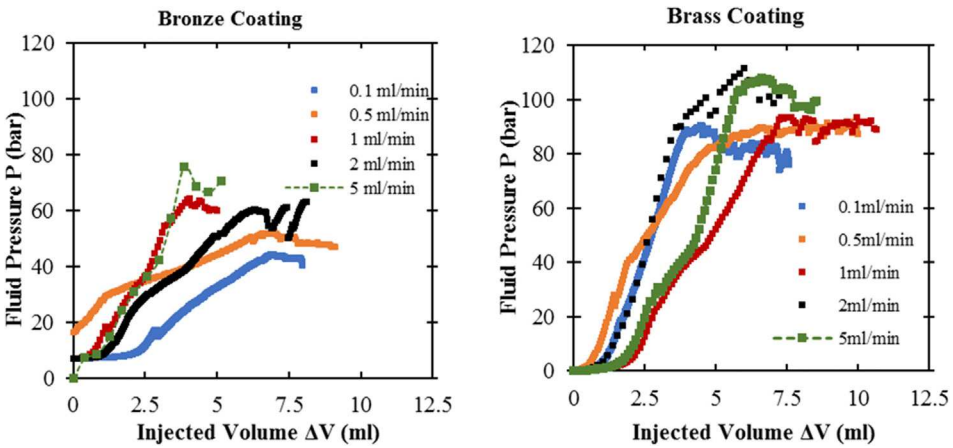

Fig. 16. RCAIT results for rubber Mix A at five different loading rates.

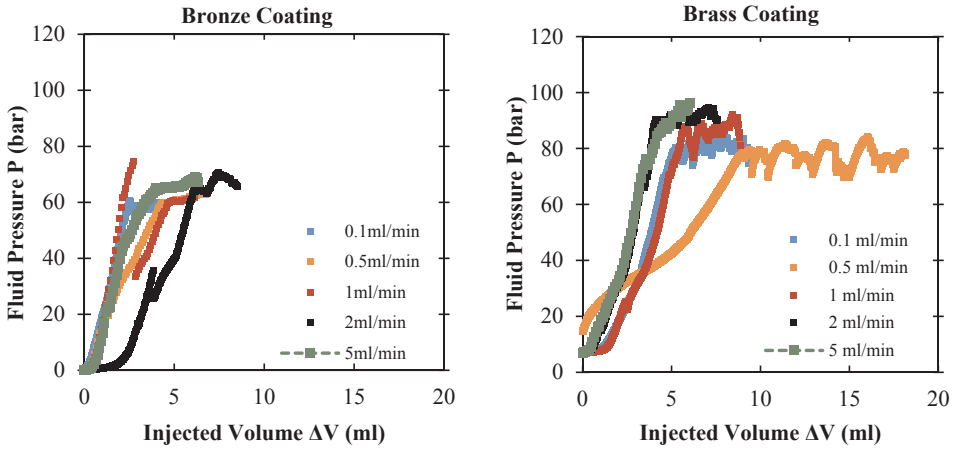

Fig. 17. RCAIT results for rubber Mix B at five different loading rates.

the onset of crack propagation. Fluid penetration at the interface can be seen in the form of fluctuations in the crack propagation pressure.

Overall, for both Mix A and Mix B, specimens with brass coated cords show higher crack propagation pressure than specimens with bronze coated cords. This difference in pressure levels is much greater for Mix A specimens than Mix B. For any given rubber

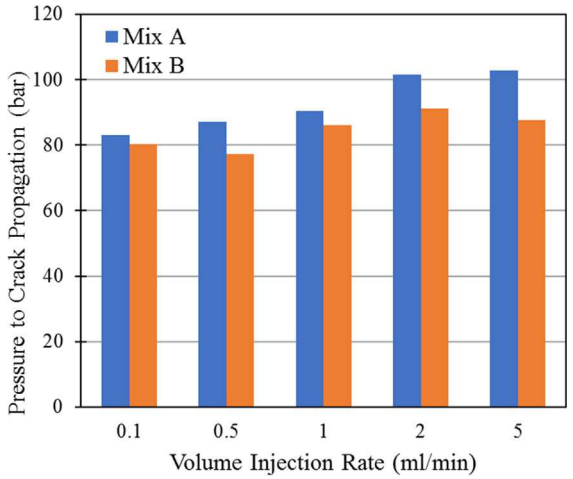

Fig. 18. Crack propagation pressure for Mix A and Mix B bonded to brass coated steel cord.

mix, the fluid volume injected during the test is slightly larger for bronze coated cords than brass coated cords.

3.2. Post-processing

Only the specimens with brass-coated cords are considered for post-processing. Bronze coated cords were used for demonstration purpose only.

A small variation in the crack propagation pressure can be observed in Fig. 18 for both rubber mixes. For rubber Mix B the pressure varies within a narrower gap than Mix A. This variation could be a mixture of dissipation at the interface as well as in the rubber. However, the dissipation in the rubber is assumed to be minor and virtually constant, based on the tensile test results. The inflation tests show similar trends to the tensile tests for both types of rubber. The rate effect is significantly smaller for Mix B. To separate the effects of the rubber from those of the interface, one should investigate the effect of volume injection rate on the crack propagation rate (V_p). The crack propagation process is a self-similar process, therefore the behaviour of rubber during crack propagation can be assumed as repetitive. The different phenomena observed are therefore a result of fluid-interface interaction.

For self-similar crack propagation, calculating the rate of crack propagation is straightforward. In Fig. 7 the time required for crack propagation over *50 mm* was *3.86* min, giving an average crack growth rate of $V_p = 12.95\ mm/\text{min}$.

The same procedure is followed for all the tests to calculate V_p. The trend visible in Fig. 19 clearly indicates the effect of volume injection rate (or in other words, fluid penetration rate). Here, an almost linear trend is observed between fluid injection and crack propagation rate. Due to the incompressible nature of the fluid (water) and a high stiffness of the test equipment, for a given system (rubber mix + cord coating type) and critical pressure value, the crack propagation rate is essentially controlled by the injection rate.

Mix B-brass coated cord specimens show higher crack propagation rates than Mix A-brass coated cord specimens (Fig. 19), reflected in Fig. 20 as lower G_c values. The error bars in Fig. 20 correspond to the standard deviation of G values based on the material parameters for five strain rates (Fig. 15).

Higher crack propagation rate is followed by greater fluid penetration. For rubber Mix A, the value of G_c doubles between the two extreme volume injection rates. There is a steady rise in the G_c values for Mix A specimens. This rise seems contradictory to the rise in V_p seen in Fig. 19. Fluid penetration is greater for large injection rates but G_c is higher as well. This suggests that the viscous dissipation at the interface is at play for higher injection rates. In the case of Mix B rubber, this effect is much weaker. In addition, if the error bars are considered, the effect of fluid injection rate on G_c for Mix B rubber specimens is even smaller.

For the rubber Mix A-brass cord specimen loaded at *1 ml*/min volume injection rate, G_c was calculated as $80.2 kJm^{-2}$. For the same case, the *Thick Rubber Tube Inflation Model* predicts $G_c = 100.6 kJm^{-2}$ (Fig. 15, Fig. 20, Table 1). The agreement is good, but the difference could be attributable to variability of G_c related to the quality of fit to the rubber model. It is also important to note that the value calculated using a more general definition of SERR does not consider various macro/microscopic phenomena such as dissipation in rubber, dissipation at the interface, fluid-rubber interaction (e.g. swelling), etc. On the other hand, the values shown in Fig. 20 are calculated based on average values of Ogden parameters obtained from the uniaxial tensile tests. Therefore, a disagreement between values of G_c calculated using the two methods is understandable.

4. Conclusion

In this work, the *Rubber Cord Adhesion Inflation Test* (RCAIT) protocol first described in [13] was studied in detail. Specifically, issues of rubber model sensitivity to the calculation of G and effect of loading rate on crack propagation were addressed.

A new *Thick Rubber Tube Inflation Model* was developed for an Ogden rubber, which can be used for other elastomeric models with slight modification. The model was extended to compute fracture energy of adhesion using a global energy balance similar to the one

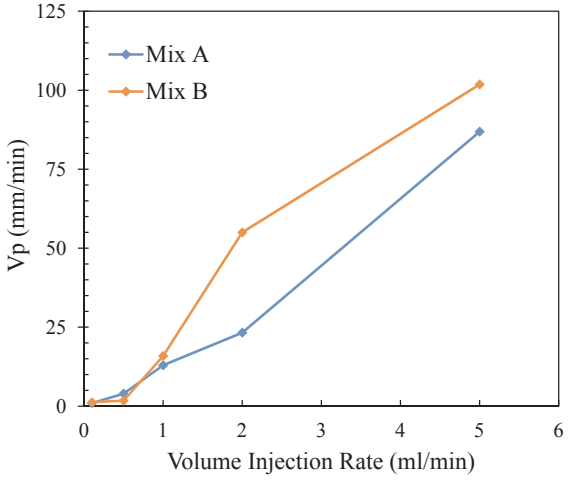

Fig. 19. Crack propagation rate Vp for Mix A and Mix B bonded to brass-coated steel cord.

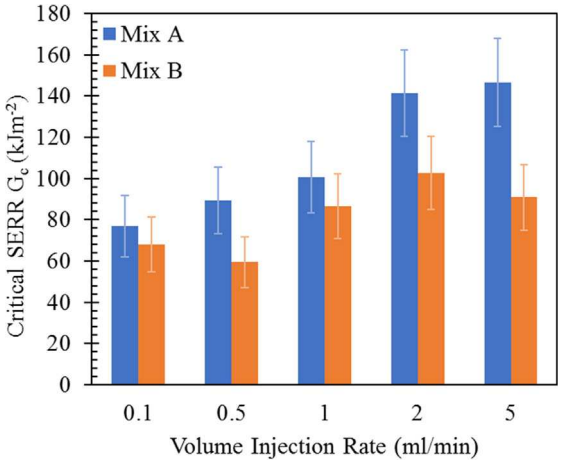

Fig. 20. G_c for 5 loading rates. The specimens consisted Mix A and Mix B bonded to brass coated cord.

Table 1
Comparison of Gc calculated using experimental data and theoretical model.

	Experiment	Theory
G_c (kJm^{-2})	80.2	100.6

described in [13]. The fracture energy equation *(19)* is a function of fluid pressure, material properties (α and μ) and specimen dimensions. By comparing the curves in Fig. 14 with a similar curve in [13], it can be concluded that the calculation of G is highly sensitive to the definition of the rubber model. By choosing a better fitting rubber model, it is possible to decouple the rubber behaviour from fracture behaviour, thereby enabling an intrinsic evaluation of the interface fracture energy. The image processing technique described here can be extended for all experiments to study crack propagation rate and its effect on fracture energy.

In the experimental part, two types of rubber mixes adhered to two types of coatings viz. brass and bronze were tested. The fluid injection rate was varied up to 50-fold and subsequent fracture behaviour was studied in detail. Increasing crack propagation pressure was observed for higher rates for all specimen types. The intensity of fluid penetration is much higher for higher injection rates; however, the fracture energy is also higher. This leads to the conclusion that loading rate effect is observed to a much larger extent than that associated with strain rate sensitivity of the mixes. However, various other factors such as swelling of rubber at such high pressures and the effect of friction between the inflating rubber and confinement tube could also affect the results.

To support such conclusions, additional investigation should now be carried out using different types of fluids and their interaction with the rubber mixes and/or the rubber-metal interface. The test developed opens the path to study the influence of liquid properties, such as surface free energy (surface tension) and intrinsic polarity, on adhesion propensity and fracture.

Declaration of Competing Interest

The authors declare that they have no known competing financial interests or personal relationships that could have appeared to influence the work reported in this paper.

Acknowledgement

The authors would like to acknowledge Maxime Daude of MFP Michelin for providing all the test specimens for RCAIT. Jeremy Guitard of I2M-University of Bordeaux is also thanked for his help in setting up the experiments.

Appendix A. Supplementary material

Supplementary data to this article can be found online at https://doi.org/10.1016/j.engfracmech.2019.106783.

References

[1] Walter JD. Cord—rubber tire composites: theory and applications. Rubber Chem Technol 1978;51(3):524–76.
[2] van Ooij WJ. The role of XPS in the study and understanding of Rubber-to-metal bonding. Surf Sci 1977;68:1–9.
[3] Cook JW, Edge S, Packham DE. The adhesion of natural rubber to steel and the use of the peel test to study its nature. Int J Adhes Adhes 1997;17(4):333–7.
[4] ASTM D1781-98, Standard Test Method for Climbing Drum Peel for Adhesives, West Conshohocken (PA): American Society of Testing and Materials; 2012.
[5] ASTM D2229-10, Standard Test Method for Adhesion Between Steel Tire Cords and Rubber, West Conshohocken (PA): American Society of Testing and Materials;

2014.
[6] ASTM D429-14, Standard test methods for rubber property – adhesion to rigid substrates, West Conshohocken (PA): American Society of Testing and Materials; 2014.
[7] Dannenberg H. Measurement of adhesion by a blister method. J Appl Polym Sci 1961;5(14):125–34.
[8] Chang YS, Lai YH, Dillard DA. The constrained blister—a nearly constant strain energy release rate test for adhesives. J Adhes 1989;27(4):197–211.
[9] Napolitano MJ, Chudnovsky A, Moet A. The constrained blister test for the energy of interfacial adhesion. J Adhes Sci Technol 1988;2(1):311–23.
[10] ASTM D1871-04, Standard Test Method for Adhesion Between Tire Bead Wire and Rubber, West Conshohocken (PA): American Society of Testing and Materials; 2014.
[11] Gent AN, Kaang SY. Pull-out and push-out tests for rubber-to metal adhesion. Rubber Chem Technol 1989;62(4):757–66.
[12] ASTM D4393-04, Standard Test Method for Strap Peel Adhesion of Reinforcing Cords or Fabrics to Rubber Compounds, West Conshohocken (PA): American Society of Testing and Materials; 2004.
[13] Kane K, Jumel J, Lallet F, Mbiakop-Ngassa A, Vacherand J-M, Shanahan MER. A novel inflation adhesion test for elastomeric matrix/steel cord. Int J Solid. Struct 2019;160: 40–50.
[14] Skala DP. Modified equations of rubber elasticity applied to the inflation mechanics of a thick-walled rubber cylinder. Rubber Chemi Technol 1970;43(4):745–57.
[15] Gent AN. Elastic instabilities in rubber. Int J Nonlin Mech 2004;40(2–3):165–75.